Journal of Crohn's and Colitis, 2023, **17**, 1471–1488
https://doi.org/10.1093/ecco-jcc/jjad064
Advance access publication 2 April 2023
Original Article

Transepithelial Barrier Dysfunction Drives Microbiota Dysbiosis to Initiate Epithelial Clock-driven Inflammation

Yu-Chen Pai,[1] Yi-Hsuan Li,[1] Jerrold R. Turner,[2] Linda Chia-Hui Yu[1]

[1]Graduate Institute of Physiology, National Taiwan University College of Medicine, Taipei, Taiwan ROC
[2]Brigham's Women Hospital, Harvard Medical School, Boston, MA, USA

Corresponding author: Linda Chia-Hui Yu, PhD, Graduate Institute of Physiology, National Taiwan University College of Medicine, Suite 1020, #1 Jen-Ai Rd. Sec. 1, Taipei 100, Taiwan ROC. Tel.: 886-2-23123456 ext. 288237; fax: 886-2-23964350; Email: lchyu@ntu.edu.tw

Abstract

Background: Factors that contribute to inflammatory bowel disease [IBD] pathogenesis include genetic polymorphisms, barrier loss, and microbial dysbiosis. A major knowledge gap exists in the origins of the colitogenic microbiome and its relationship with barrier impairment. Epithelial myosin light chain kinase [MLCK] is a critical regulator of the paracellular barrier, but the effects of MLCK activation on the intraepithelial bacteria [IEB] and dysbiosis are incompletely understood. We hypothesise that MLCK-dependent bacterial endocytosis promotes pathobiont conversion and shapes a colitogenic microbiome.

Methods: To explore this, transgenic [Tg] mice with barrier loss induced by intestinal epithelium-specific expression of a constitutively active MLCK were compared with wild-type [WT] mice.

Results: When progeny of homozygous MLCK-Tg mice were separated after weaning by genotype [Tg/Tg, Tg/WT, WT/WT], increased IEB numbers associated with dysbiosis and more severe colitis were present in Tg/Tg and Tg/WT mice, relative to WT/WT mice. Cohousing with MLCK-Tg mice induced dysbiosis, increased IEB abundance, and exacerbated colitis in WT mice. Conversely, MLCK-Tg mice colonised with WT microbiota at birth displayed increased *Escherichia* abundance and greater colitis severity by 6 weeks of age. Microarray analysis revealed circadian rhythm disruption in WT mice co-housed with MLCK-Tg mice relative to WT mice housed only with WT mice. This circadian disruption required Rac1/STAT3-dependent microbial invasion but not MLCK activity, and resulted in increased proinflammatory cytokines and glucocorticoid downregulation.

Conclusions: The data demonstrate that barrier dysfunction induces dysbiosis and expansion of invasive microbes that lead to circadian disruption and mucosal inflammation. These results suggest that barrier-protective or bacterium-targeted precision medicine approaches may be of benefit to IBD patients.

Key Words: Epithelial barrier; microbiome; invasive pathobionts; circadian rhythm; epithelial glucocorticoid; enterocolitis

Graphical Abstract

Transepithelial barrier dysfunction drives microbiota dysbiosis to initiate epithelial clock-driven inflammation

Yu-Chen Pai[1], Yi-Hsuan Li[1], Jerrold R. Turner[2], and Linda Chia-Hui Yu[1]*

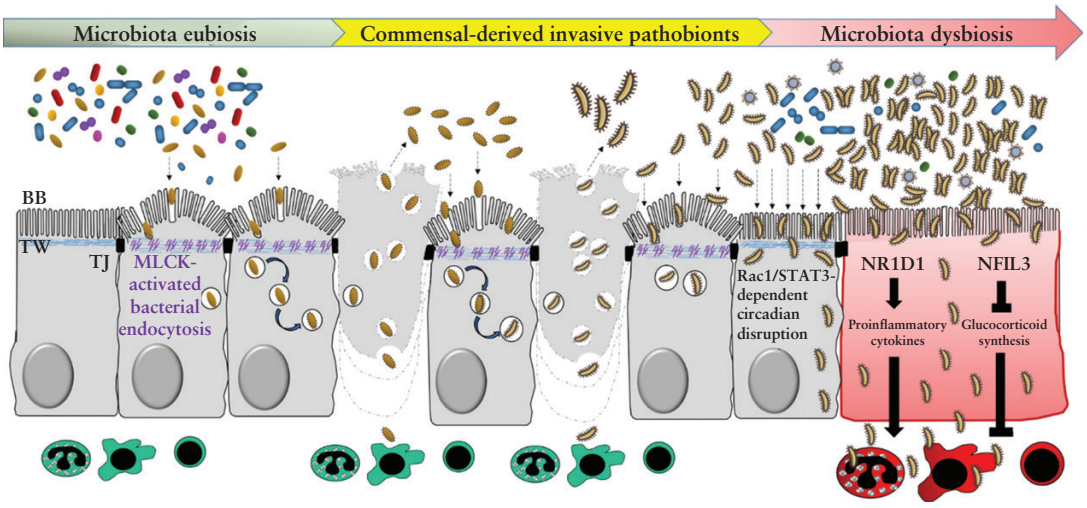

1. Introduction

The aetiology of inflammatory bowel diseases [IBDs] is complex, as host genetics, intestinal microbiome, barrier dysfunction, and immune hyperactivation contribute to disease development. Elevated intestinal permeability, before either disease onset or symptom flare,[1–3] increased numbers of mucosa-associated bacteria,[4,5] and altered microbiota composition[6,7] have been described in IBD patients. These changes are also present in animal models of colitis.[8,9] Our previous work has shown that the endocytosis of commensal bacteria proceeds increased tight junction permeability in mouse models of enterocolitis, and that inhibition of epithelial barrier loss prevents mucosal inflammation.[10–12] The observation that transplantation of a dysbiotic microbiome from IBD patients triggers colitis in germ-free mice indicates a critical role for gut microbes.[13,14] Nevertheless, the origins of disease-associated dysbiosis and its relationship with gut barrier loss remain poorly understood.The gut microbiome is initially provided at birth and is then shaped by factors that include diet, immune signalling, and antimicrobial peptides.[15,16] However, the means by which the microbiota are converted from eubiosis to the dysbiosis associated with colitis are still unknown. An altered microbiome has been associated with increased colitis susceptibility in mice lacking innate immune receptors including nucleotide-binding oligomerisation domain [NOD]-like receptors NOD2 and NLRP6, but it was not clear if the dysbiosis was a consequence of immune defects. Cross-fostering studies confirmed that the microbiota of innate immune receptor-deficient mice was maternally derived but did not reveal the cause of dysbiosis.[17,18] Further, adherent-invasive *Escherichia coli* [AIEC] isolated from Crohn's disease patients aggravated experimental colitis,[19,20] supporting the existence of pathobionts [opportunistic pathogens derived from commensals] in the intestine. Nevertheless, the processes by which these create dysbiosis remain undefined.

Intestinal epithelial barrier loss and increased intraepithelial bacteria [IEB] abundance can reflect either endocytosis or active invasion. We and others have previously shown that MLCK expression is upregulated[21,22] and associated with increased IEB numbers in colon biopsies from IBD patients.[4,5] Further, we used knockout mice that lack epithelial MLCK and pharmacological inhibitors to demonstrate that induction of bacterial internalisation is one means by which MLCK enhances the pathogenesis of colitis. This reflects the terminal web actomyosin contraction and brush border fanning, which facilitate caveolae-dependent bacterial endocytosis through cholesterol-rich lipid rafts as a consequence of MLCK activation.[10–12] Other epithelial responses, including innate immune signalling, can also modify proinflammatory cytokine production *in vitro*, and epithelium-specific deficiency of Toll-like or NOD-like receptor exacerbates colitis *in vivo*.[23–26] Conversely, bacteria adapt to stressful environments such as intracellular niches to ensure survival.[27,28] We hypothesised that endocytosis of commensal bacteria might facilitate emergence of invasive pathobionts and promote the shaping of a colitogenic microbiome.

In the current study, transgenic mice [MLCK-Tg] that express constitutively active MLCK specifically within intestinal epithelia were compared with wild-type [WT] mice. Numbers of IEB, microbiota composition, and colitis severity were compared under single- and co-housed conditions. Further, we used a new strategy in which MLCK-Tg neonates are colonised with a WT microbiome to elucidate processes responsible for conversion of the microbiome from eubiosis to dysbiosis. We identified molecular mechanisms of bacterial endocytosis, pathobiont invasion, and disruption of epithelial circadian rhythm as a consequence of colonisation by a MLCK-Tg microbiome.

Methods

Approval for the animal study was granted by the Institutional Animal Care and Use Committee of NTUCM [IACUC#20201051].

2.1. Animals

Transgenic [MLCK-Tg] mice expressing constitutively active MLCK specifically within intestinal epithelia were generated as described.[29,30] The MLCK-Tg and wild-type C57BL/6 [WT] mice were bred as homozygotes and conventionally raised in a specific pathogen-free environment in the animal facility. All animals were housed in a temperature-controlled room with 12-h light-dark cycles, and fed regular chow and water. The animal studies were approved by the Institutional Animal Care and Use Committee of NTUCM.

2.2. Breeding and housing conditions

Mice were bred and either single-housed [SIN], co-housed [COH], or aggregated on the basis of littermate genotype-based separation [LGS]. For the SIN and COH studies, MLCK-Tg and WT mice were conventionally raised by homozygous breeding pairs for over five generations. The pups generated were nursed by their biological mothers, weaned at 3 weeks of age, and used at up to 10 weeks of age for experiments under SIN conditions. In parallel, homozygous mice were subjected to COH conditions, beginning at 4 weeks of age, by co-housing MLCK-Tg and WT mice. Tissues and faecal samples were aseptically collected from 8–10 week-old mice under SIN and COH conditions. Only male mice were used for the SIN and COH studies. A new strategy in which both dam and sire were hemizygous for MLCK-Tg but nursed only by WT dams was employed to ensure comparable intrauterine environments and postnatal delivery of WT maternal microflora to all pups, regardless of genotype. Littermates of each genotype [Tg/Tg, Tg/WT, WT/WT] were caged separately [LGS] after weaning. Faecal and epithelial samples were collected aseptically from each mouse at 3, 6, and 10 weeks of age. Samples obtained from 3-week old neonates [both female and male] nursed by WT dams in the same cage represented the pre-weaning microbiome, and samples obtained from male mice at 6 and 10 weeks of age were representative of separately caged adults consuming normal chow.

2.3. Colitis models

For up to 7 days, 8–10-week old mice received 2.5% dextran sodium sulphate [DSS; MP Biomedicals] in the drinking water. Alternatively, mice received intracolonic instillation of 2,4,6-trinitrobenzene sulphonic acid solution [TNBS; Sigma] at 25 mg/kg dissolved in 40% ethanol for one bolus, and were euthanised 6 h later. Age-matched mice that were not administered colitogenic agents were used as untreated controls. All mice were euthanised between 10:00 and 14:00 [unless otherwise stated] for quantitative analyses of IEB. Gene expression

was analysed in purified epithelial cells [see below] by quantitative polymerase chain reaction [qPCR] analysis using primer pairs designed in this study [Supplementary Table 1]. Colitis severity was assessed by measuring histopathological scores and myeloperoxidase [MPO] activity, indicative of neutrophil infiltration.[10] Cytokine profiles and glucocorticoid-related enzyme levels were also determined in mucosal tissues, using commercial enzyme-linked immunosorbent assay [ELISA] kits and qPCR analysis.

2.4. Broad-spectrum antibiotics treatment in mice

Broad-spectrum antibiotics [ABX] mixtures [vancomycin 500 mg/L, neomycin 1 g/L, metronidazole 1 g/L, and ampicillin 1 g/L] were orogavaged daily and added into drinking water for 1 week prior to the administration of colitogenic agents.

2.5. *In vivo* infection of mouse-isolated bacteria

For 11 days, 8-week old mice were administered 1.5% DSS in the drinking water and gavaged with phosphate-buffered saline [PBS] or 10^8 colony-forming units [CFUs] of bacteria each day for 9 days.[31] In some experimental settings, mice were administered 5 mg/kg NSC23766 [a specific Rac1 inhibitor] by intraperitoneal injection 1 h before bacterial gavage.

2.6. Isolation of purified epithelial cells for gentamicin resistance assay

Intestinal segments [10-cm] were excised and flushed with PBS for epithelial cell isolation as previously described.[10–12,32–34] The segments were inverted on a steel rod with a diameter of 3 mm, and immersed in 5.56 mM glucose in PBS [PBS-G] containing 0.5 mM dithiothreitol [DTT] for 10 min at room temperature to remove mucus. The inverted intestines were then placed in PBS-G with 30 mM ethylenediaminetetraacetic acid [EDTA] for 30 min at 37°C with gentle shaking. The cell suspension was poured through a mesh filter [40-μm pore size], and the epithelial cells left on the mesh were collected by eluting the inverted filter with PBS-G. The cell pellet after centrifugation was resuspended in PBS-G solution, and the numbers of trypan-blue negative cells were determined. Our pilot studies had shown that cell viability was 92.7 ± 0.3%, and the purity of epithelial cells was 91.1 ± 1.2% as determined by BerEP4-positivity by flow cytometry. The purified epithelial cells [2×10^6] were incubated with 300 μg/mL gentamicin [Sigma] for 1 h with gentle shaking. After PBS washing twice, cells were lysed with 1% Triton X-100 in PBS for 10 min on ice. Subsequently, the cell lysate [200 μl] was plated onto fresh blood agar plates for bacterial culturing overnight at 37°C. The colonies were counted and the intracellular bacterial counts presented as $\log_{10}$ CFU per 10^6 cells.

2.7. Characterisation of intraepithelial bacteria

Bacteria were cultured on blood agar plates, and DNA from individual colonies was extracted for the classification using 16S rDNA sequencing. The antibiogram analysis of bacteria was performed in the Department of Laboratory Medicine in National Taiwan University Hospital [NTUH]. All bacteria showed susceptibility to gentamicin with a minimum inhibitory concentration of 2 μg/ml.

2.8. Faecal and epithelial microbiota analysis

Bacterial DNA was extracted from faecal samples and mouse colonic epithelial cells. High-throughput 16S rDNA sequencing was performed using the PacBio Sequel II or Illumina Genome Analyzer IIx platform. Microbial operational taxa units [OTUs] were used for alpha rarefaction analysis to determine the diversity within a community by calculating the Shannon index, which estimates species richness. The beta rarefaction analysis that determines the diversity between samples was conducted by algorithms of the weighted UniFrac method.[33]

2.9. Genome-wide microarray

Tissue RNA was extracted using a RNeasy Mini Kit [Qiagen] and sent for microarray analysis using the Clariom™ S Assay to analyse more than 22 100 mouse genes at the National Health Research Institute [Miao-Li, Taiwan]. Single-stranded cDNA was generated from the amplified cRNA with the WT Amplification Kit [Affymetrix] and then fragmented and labelled with the WT Terminal Labeling Kit [Affymetrix]. Samples were hybridised with probes of Clariom™ S Assay, mouse arrays, and scanned using a gene microarray device [Affymetrix]. Raw data were processed with background correction and normalisation, and data analysis was performed by Transcriptome Analysis Console [TAC] 4.0. The gene array data were submitted to the GEO repository.

2.10. Macromolecular permeability tests and tight junctional assays

Intestinal tissues were mounted in Ussing chambers to measure electrophysiological parameters and luminal-to-basal flux of dextran probes [MW 4000].[10–12] Mucosal protein samples were subjected to Western blotting for occludin cleavage.[10–12]

2.11. Reagents

Pharmacological inhibitors, including ML-7 [an MLCK inhibitor; 20 μM], NSC23766 [a specific Rac1 inhibitor; 50 μM], Y27632 [a ROCK inhibitor; 20 μM], and filipin [10 μM] and methyl β-cyclodextrin [50 mM] [cholesterol-sequestering agents], were used. All reagents were purchased from Sigma.

2.12. Bacteria-epithelial cocultures

Human Caco-2 cells were exposed to bacteria in antibiotic-free culture media as described.[10,11,33] Briefly, bacteria were added to the apical side of the confluent epithelial monolayer at multiplicity-of-infection [MOI] = 100 for 1 h. The monolayer was then treated with EDTA to obtain single cells for incubation in gentamicin-containing media for 1 h. Cells were then lysed with 1% Triton X-100, and the lysate plated on agar for quantitative analysis of viable intracellular bacteria. For qPCR analyses, bacteria were incubated with epithelial cells for 1 h and then RNA was extracted from the epithelial cells [Supplementary Table 2]. For Western blotting, bacteria were incubated with epithelial cells for 1 h and replaced with gentamicin-containing media for 6 h. After rinsing with PBS, protein was extracted from the epithelial cells as described.[35]

2.13. Constructs of plasmid vectors for gene overexpression and knockdown

Caco-2 cells were plasmid transfected to overexpress genes or infected with lentiviral particles delivering short hairpin [sh] RNA to knockdown target genes following established protocols.[10,33,36,37]

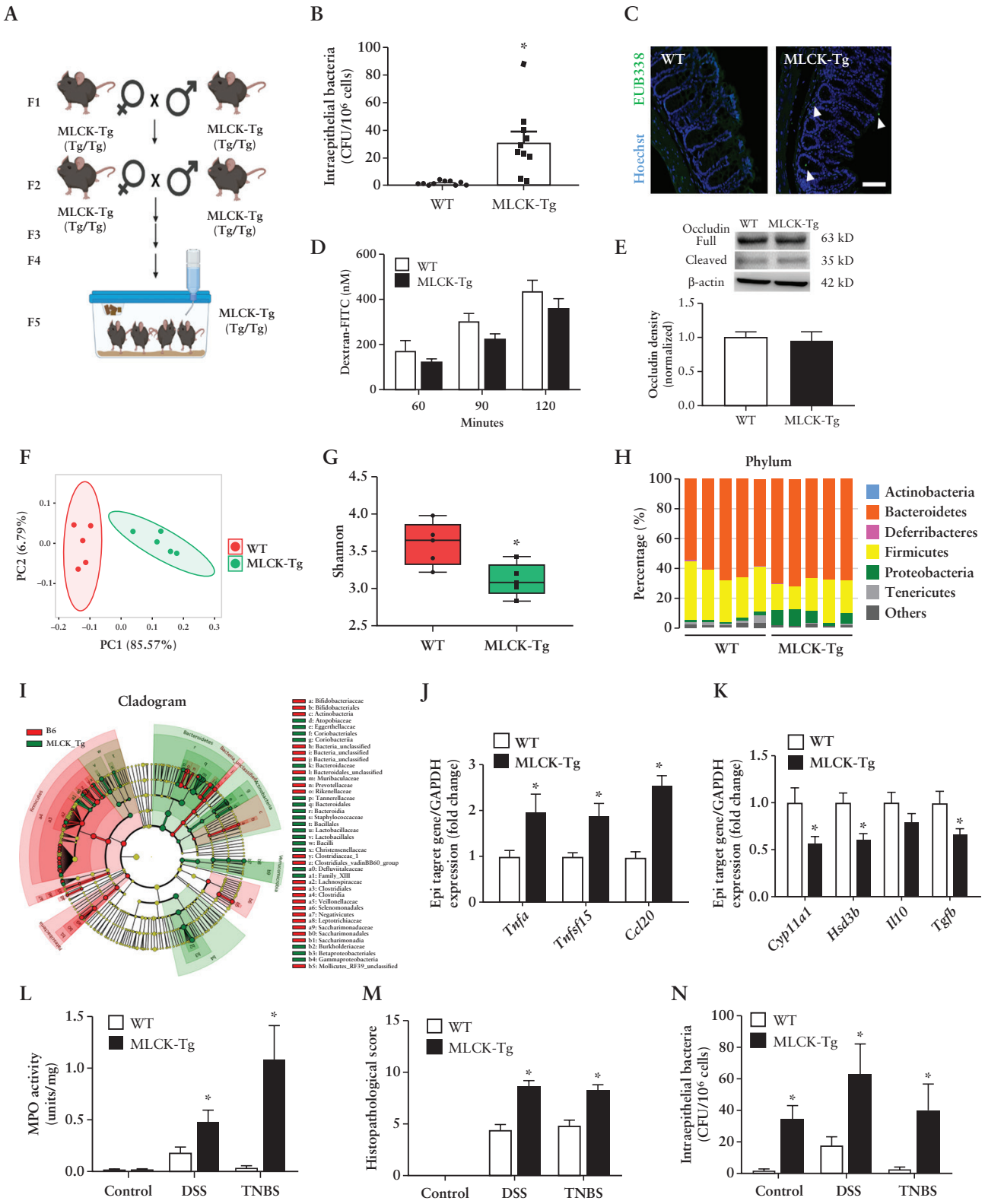

Figure 1. Coexistence of intraepithelial microbes and altered microbiota in colitis-prone MLCK-Tg mice. Gut barrier function and microbiota composition were assessed in MLCK-Tg mice and WT mice. [A] Schematic diagram using homozygous breeding pairs for generating MLCK-Tg mice over five generations. The WT mice were conventionally raised using the same method. [B] Intraepithelial bacterial [IEB] counts in mouse colonocytes at steady-state. $N = 10$/group, $^*p < 0.05$ vs. WT. [C] Presence of bacteria in the colonic epithelial layers of MLCK-Tg mice visualised by fluorescence *in situ* hybridisation. Experiments were repeated twice. Bar: 100 μm. [D] No difference in dextran flux of intestinal tissues at steady-state. [E] Western blotting of occludin shows no difference in expression. [F] Faecal microbiota analysis using full-length 16S rDNA sequencing revealed distinct composition between MLCK-Tg and WT mice. WT [red]; MLCK-Tg [green]. $N = 5$/group. [G] Lower Shannon index was observed in the faecal microbiota of MLCK-Tg compared with WT mice. [H] Percentages of faecal bacterial phyla. [I] Linear discriminant analysis effect size [LEfSe] analysis depicted by a cladogram

2.14. Epithelial glucocorticoid production

A luciferase reporter assay was conducted to assess glucocorticoid secretion due to the limited glucocorticoid synthesis by intestinal epithelia.[38,39] HEK293T cells were transfected with plasmids carrying human GR [pcDNA3.1-GR], pGL3-GRE-Luc, and pGL4.74-hRluc, using jetPRIME® Transfection reagents, and placed in a 37°C incubator for 24 h. Transfection medium was replaced by conditioned medium from Caco-2 cells. The conditioned medium was collected from Caco-2 cells that had been transfected with pcDNA3.1-NFIL3 or pLKO.1-NFIL3 for 48 h. After incubation, HEK293 cells were lysed and luciferase production assessed using a Dual-Glo Luciferase assay and microplate luminometer.

2.15. Bacterial culture and storage

Single bacterial colonies were amplified and the pellet was mixed with glycerol for storage at -80°C until use. The phylogroups of *E. coli* were determined using the Clermont method of triplex PCR assay [Supplementary Table 3].[40]

2.16. Statistical analysis

All data are expressed as the mean ± standard error of the mean [SEM] in bar graphs. Dot plots are used for bacterial counts. Data were compared by one-way analysis of variance [ANOVA] with Newman-Keuls post hoc test or by Student's t test [GraphPad Prism v.8]. For comparing differences between bacterial CFU values, the Kruskal-Wallis test or Mann-Whitney U test was used. A probability value <0.05 was considered to be significant.

Detailed methods are included in the Supplementary Material and Methods.

3. Results

3.1. Intraepithelial microbes and dysbiosis are induced by epithelial barrier loss

Our previous studies demonstrated that MLCK-activated transepithelial bacterial internalisation contributed to colitis development.[10,11] Here, IEB counts and microbiota composition of intestinal epithelium-specific, homozygous MLCK-Tg mice [Figure 1A][29,30] were compared with WT mice. The IEB counts were greater in MLCK-Tg mice relative to WT mice [Figure 1B], indicating the presence of viable intracellular microbes in MLCK-Tg colonocytes at baseline. 16S rDNA sequencing showed the presence of *Escherichia, Lactobacillus, Staphylococcus,* and *Paenibacillus* in colonocytes. The bacteria within MLCK-Tg colonocytes could also be detected by fluorescent *in situ* hybridisation [Figure 1C]. In contrast, IEB was not detected in WT mice by culture or by fluorescent *in situ* hybridisation [Figure 1B and C]. Expression of the tight junction protein occludin and luminal-to-serosal macromolecular flux in colonic tissues was similar between MLCK-Tg and WT mice [Figure 1D and E].

Principal coordinate plot [PCoA] analysis of faecal microbial 16S rDNA revealed distinct microbial communities in WT and MLCK-Tg mice [Figure 1F]. Shannon diversity was reduced in MLCK-Tg mice, relative to WT mice [Figure 1G]. In each mouse, the microbiota included six main phyla, of which Bacteroides and Firmicutes dominated [Figure 1H]. However, linear discriminant analysis effect size [LEfSe] analysis depicted by a cladogram detected significant differences in faecal bacterial populations of the two mouse genotypes [Figure 1I; and Supplementary Figure 1A and 1B]. Predicted Kyoto Encyclopedia of Genes and Genomes [KEGG] pathway, based on the faecal microbiota composition, implicated higher membrane transport and cell motility in the MLCK-Tg mice compared with WT mice [Supplementary Figure 1C]. Thus, in addition to IEB, the overall composition of the gut microbiome was altered in MLCK-Tg mice.

Pro- and anti-inflammatory cytokine expression in colonocytes was assessed by qPCR. Expression of cytokines, including tumor necrosis factor-alpha [*Tnfa*], TNF-like 1A [*Tnfsf15*], and chemokine C-C motif ligand 20 [*Ccl20*], was increased in MLCK-Tg mice relative to WT mice [Figure 1J]. In contrast, expression of glucocorticoid-related enzymes, including cytochrome P450 family 11 [*Cyp11a1*] and hydroxysteroid dehydrogenase 3-beta [*Hsd3b*], as well as tumour growth factor beta [*Tgfb*], was greater in WT mice [Figure 1K].

Colitis susceptibility was assessed using DSS or TNBS. Pilot studies confirmed that treatment conditions induced mild inflammation without overt epithelial shedding [Supplementary Figure 2A–C]. Despite cytokine differences, colonic MPO activity was comparable in control MLCK-Tg and WT mice [Figure 1L]. However, colitis was associated with greater colonic MPO activity increases as well as more advanced histological damage in MLCK-Tg mice relative to WT mice treated with DSS or TNBS [Figure 1L and M; and Supplementary Figure 2D]. Moreover, IEB numbers were increased in both genotypes after induction of colitis, but levels were higher in MLCK-Tg mice relative to WT mice [Figure 1N].

3.2. Microbiota from MLCK-Tg mice induce IEB and exacerbate colitis in WT mice

To determine whether the increased severity of colitis in MLCK-Tg mice depended on the microbiome, mice were treated with broad-spectrum antibiotics. Antibiotic treatment attenuated DSS- and TNBS-induced colitis by depleting microbial counts in the faecal and epithelial compartments [Figure 2A and B]. Thus, the microbiota of MLCK-Tg mice contain a crucial factor that exacerbates disease. Nevertheless, the relationship between barrier dysfunction and microbial alterations could not be clarified using conventionally raised mice.

To determine whether an altered microbiome alone, without barrier dysfunction, could enhance colitis severity, WT mice were co-housed [COH] with MLCK-Tg mice before treatment with DSS or TNBS. As a control, COH mice

revealed bacterial differences in the MLCK-Tg and WT mice. [J and K] Higher epithelial proinflammatory cytokines and lower epithelial anti-inflammatory mediator levels in MLCK-Tg mice compared with WT mice. *$p < 0.05$ vs. WT. [L] Negligible levels of colonic MPO activity were observed in WT and MLCK-Tg mice at steady state, but MLCK-Tg mice exhibited higher MPO activity than WT mice after administration of DSS or TNBS. The untreated control group was not administered colitogenic agents. [M and N] Histopathological scores and IEB counts in mouse colon after DSS and TNBS treatment. $N = 10$-12/group. *$p < 0.05$ vs. WT. WT, wild type; MPO, myeloperoxidase; DSS, dextran sodium sulphate; TNBS, trinitrobenzene sulphonic acid; IEB, intraepithelial bacteria.

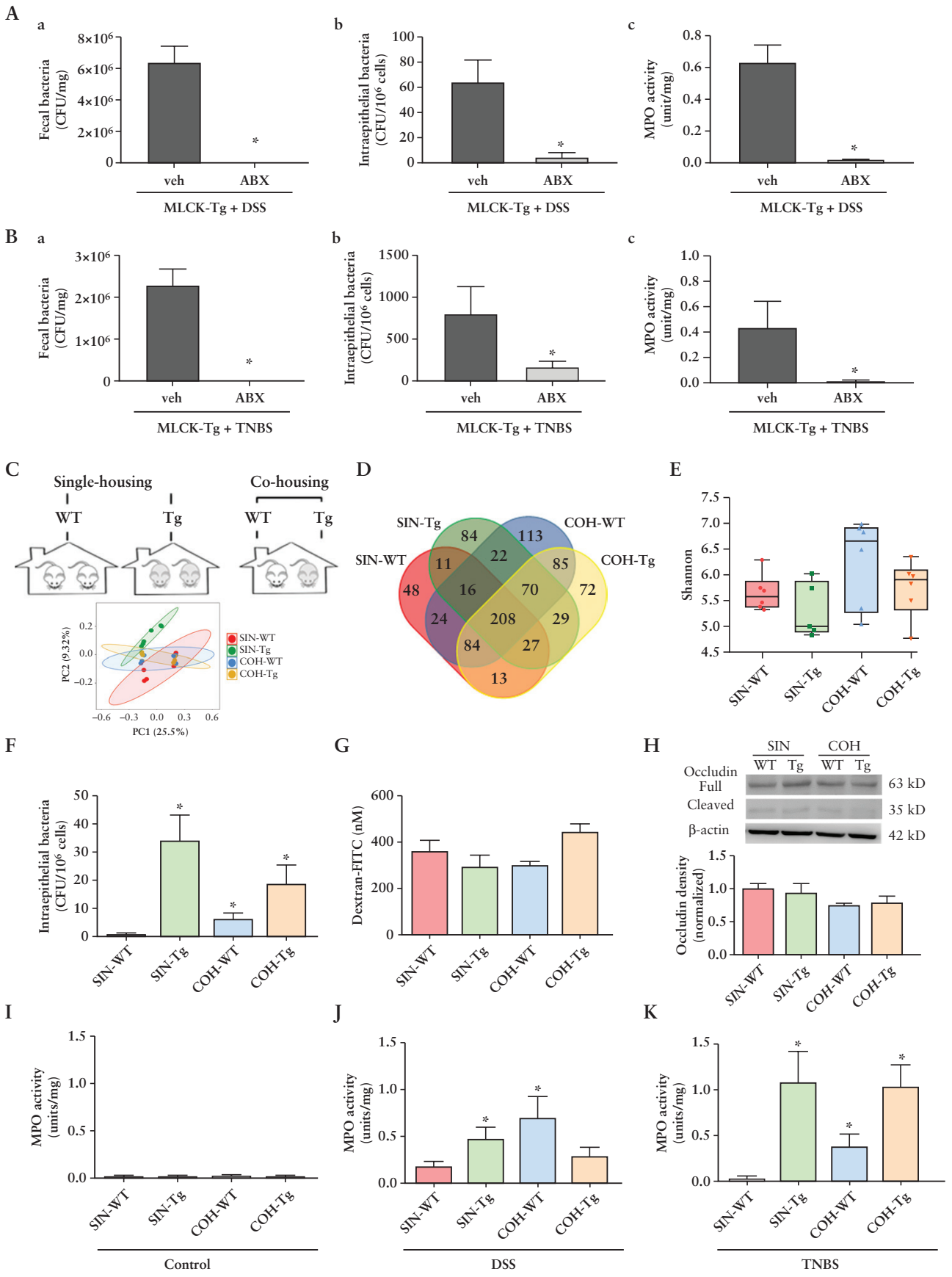

Figure 2. Dysbiotic microbiota from MLCK-Tg mice causes emergence of IEB and exacerbates colitis in the co-housed WT mice. [A and B] Broad-spectrum antibiotic [ABX] treatment decreased [a] faecal bacterial numbers, [b] IEB counts, and [c] colitis severity in the MLCK-Tg mice administered

were compared with single-housed [SIN] mice [Figure 2C]. As expected, the faecal microbiome of SIN-WT and SIN-Tg mice differed, but co-housing resulted in clustering of bacterial populations and increased numbers of overlapping OTUs between genotypes, likely as a result of coprophagy [Figure 2C–E]. LEfSe analysis confirmed significant changes in microbiome composition after co-housing [Supplementary Figure 3].

IEB numbers were increased in colons of COH-WT mice relative to SIN-WT mice [Figure 2F], suggesting invasive bacteria within the MLCK-Tg microbiome. In comparison, numbers of IEB were negligible in epithelial cells of SIN-WT mice. Genera of IEB that emerged in the COH-WT mice included *Escherichia, Lactobacillus, Staphylococcus,* and *Paenibacillus*. In contrast, COH-Tg mice and their SIN-Tg counterparts had similar IEB numbers [Figure 2F]. Moreover, comparable occludin levels and dextran flux were observed in the colonic tissues across the four groups at baseline [Figure 2G and H].

Despite increased IEB numbers, MPO remained undetectable in both genotypes under SIN or COH conditions [Figure 2I]. However, colonic MPO activity was greater in DSS- or TNBS-treated COH-WT mice relative to DSS- or TNBS-treated SIN-WT mice [Figure 2J-K]. Correspondingly, mucosal IFNγ and IL-17 were also greater in COH-WT mice than in SIN-WT mice treated with colitogenic agents [Supplementary Figure 4A, B]. Thus, co-housing with MLCK-Tg mice induced IEB and increased colitis severity in WT mice.

3.3. MLCK-dependent bacterial endocytosis shapes the faecal microbiome to cause dysbiosis

Although co-housing with MLCK-Tg mice induced faecal dysbiosis in WT mice, the processes responsible for a colitogenic microbiome containing invasive microbes in MLCK-Tg mice remained unclear. We speculated that the intraepithelial environment might serve as a stressor that evokes conversion of internalised commensal microbes into invasive pathobionts. However, this hypothesis could not be explored using the current breeding strategy, as the colitogenic microbiota of MLCK-Tg mice are likely maternally acquired.

The hypothesis above was tested using a novel breeding strategy that allowed newborn MLCK-Tg mice to be colonised by a WT microbiome [Figure 3A]. Simply, hemizygous [Tg/WT] mice were bred to generate Tg/Tg, Tg/WT, and WT/WT pups. These were transferred to and nursed by WT dams immediately after birth in order to ensure colonisation by a WT maternal microbiome. At weaning, littermate genotype-based separation [LGS] was employed to house mice in groups according to genotype [Figure 3A].

Just prior to weaning, at 3 weeks of age, 16S rDNA sequencing data failed to detect differences between the epithelial or faecal microbiota of each genotype [Figure 3B-a, C-a]. Thus, littermates raised by WT dams harboured comparable microbiota within both epithelial and faecal compartments prior to weaning. In contrast, the epithelial microbiome of LGS[Tg/Tg] and LGS[WT/WT] mice diverged by 6 weeks of age [Figure 3B-b]. This difference remained at 10 weeks of age [Figure 3B-c]. In contrast, the faecal microbiome of LGS[Tg/Tg] and LGS[WT/WT] mice did not divert until 10 weeks of age [Figure 3C], suggesting that the epithelial microbiome dictates the composition of the faecal microbiome rather than vice versa. Further, these data show that epithelial MLCK activation is responsible for the observed genotype-specific microbiome differences in adulthood.

At 3 weeks of age, high numbers of IEB were present in colonocytes of all mice, regardless of genotype [Figure 3D]. Although IEB abundance decreased dramatically by 6 weeks of age in all genotypes, IEB numbers were significantly greater in LGS[Tg/Tg] mice relative to LGS[WT/WT] mice [Figure 3D]. Notably, the dramatically increased IEB numbers at 3 weeks of age do not reflect gross barrier defects or changes in occludin expression [Figure 3E].

Shannon diversity of epithelial microbiota was high in 3-week old mice, regardless of genotype [Figure 3F]. The data were consistent with the findings of leakiness of neonatal immature gut.[41,42] Even at this early time point, diversity of the epithelial microbiome was greater in LGS[WT/WT] relative to corresponding LGS[Tg/WT] and LGS[Tg/Tg] groups [Figure 3F], suggesting enrichment of particular intracellular bacteria due to epithelial MLCK activation. Moreover, a 5.6-fold increase in *Escherichia* abundance was already present in the epithelial microbiota of 3-week old LGS[Tg/Tg] relative to LGS[WT/WT] [Figure 3G and H]. Similar changes, such as a 2-fold enrichment in *Escherichia*, were also present in the faecal microbiome of 3-week old LGS[Tg/Tg] relative to LGS[WT/WT] [Figure 3G and H]. Composition of both epithelial and faecal microbiota continued to evolve after weaning, and differences were noted in the 6- and 10-week old mice [Supplementary Figure 5A–D].

DSS- and TNBS-induced colitis was more severe in adult LGS[Tg/Tg] mice relative to LGS[WT/WT] mice, as measured by MPO activity [Figure 3I–K], mucosal IFNγ and IL-17 production [Supplementary Figure 4C, D], and histopathological mucosal damage [Supplementary Figure 4E]. Overall, the IEB counts and divergence of the epithelial and faecal microbiota correlated positively with colitis severity across the mouse genotypes. The data suggested that the enrichment

DSS or TNBS. $N = 6$–9/group. *$p < 0.05$ vs. vehicle. [C] Schematic diagram of the housing conditions, including single-housed [SIN] and co-housed [COH] settings for conventionally raised mice. WT mice with intact gut barriers were subjected to cohousing with MLCK-Tg mice to evaluate the transmissibility of dysbiotic microbiota for modulating colitis susceptibility. The PCoA analysis revealed distinct faecal microbiota in the SIN-WT and SIN-Tg mice, and a proximate bacterial composition in the COH-WT and COH-Tg mice, which confirmed coprophagy by co-housing. $N = 3$/group. Experiments were repeated twice. [D] Venn diagrams of differential bacterial compositions in faecal microbiota. Co-housing led to 447 operational taxonomic units [OTUs] overlapping between MLCK-Tg and WT mice compared with only 262 OTUs in their SIN counterparts. [E] Shannon index of faecal microbiota was comparable between COH-WT and COH-Tg mice. $N = 6$/group. [F] Higher IEB counts were observed in the colonocytes of COH-WT mice relative to SIN-WT mice. The emergence of IEB in the WT recipients implicated the transfer of invasive microbes from MLCK-Tg mice. $N = 10$–12/group. *$p < 0.05$ vs. SIN-WT. [G and H] No difference in luminal-to-serosal dextran flux or occludin cleavage was observed in mouse intestinal tissues under SIN or COH conditions. [I] Negligible MPO activity in untreated control mice under SIN or COH conditions. [J and K] Higher MPO activity was found in COH-WT mice than in SIN-WT mice after DSS and TNBS treatment, indicating that dysbiotic microbiota from MLCK-Tg mice exacerbated colitis in the co-housed WT recipients. $N = 10$–12/group. *$p < 0.05$ vs. SIN-WT. WT, wild type; MPO, myeloperoxidase; DSS, dextran sodium sulphate; TNBS, trinitrobenzene sulphonic acid; IEB, intraepithelial bacteria; PCoA, principal coordinate analysis.

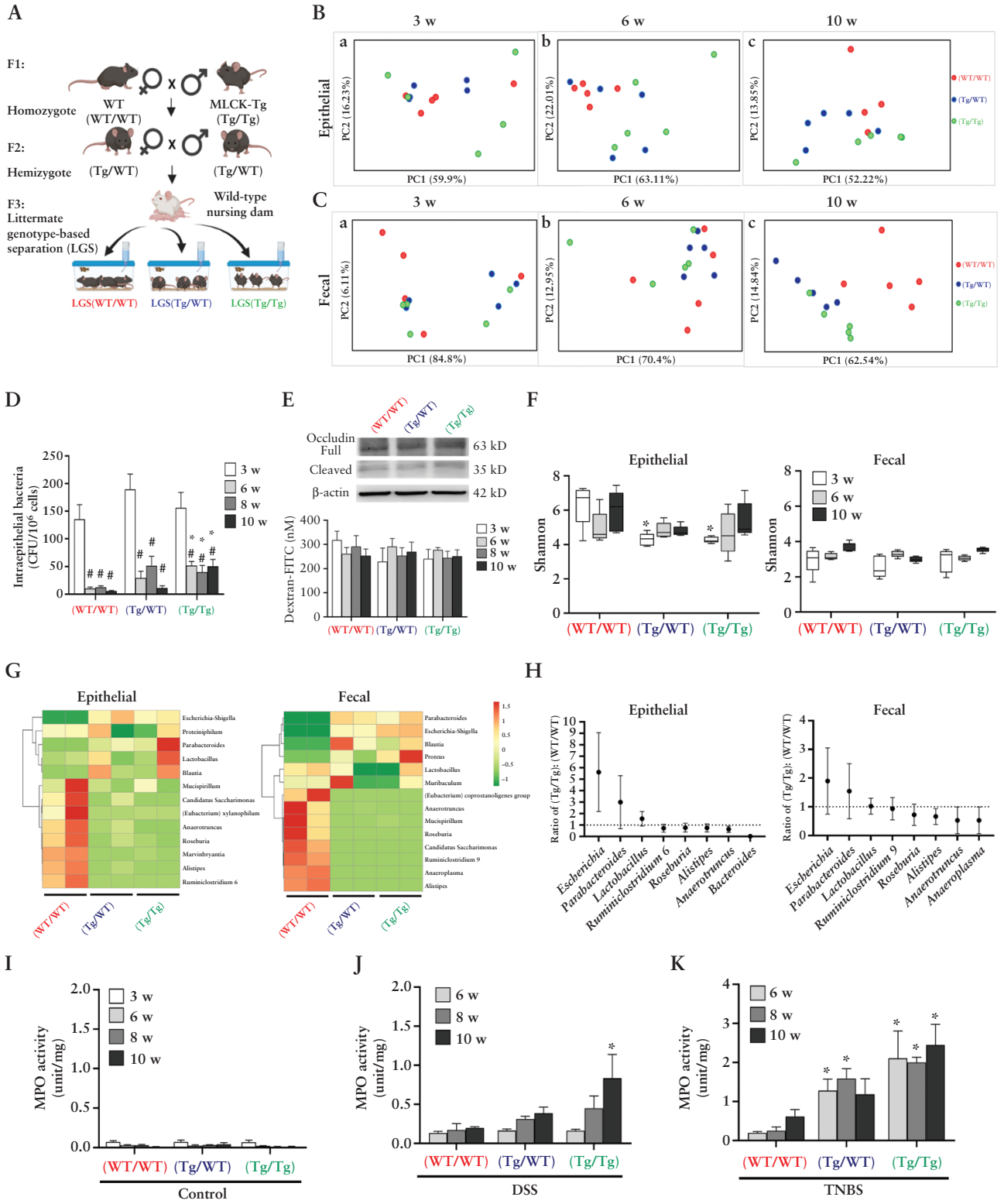

Figure 3. Epithelial MLCK-activated bacterial internalisation plays a causative role in microbiota conversion from eubiosis to dysbiosis. A novel breeding strategy was employed to achieve neonatal colonisation of WT microbiota in MLCK-Tg pups in order to assess the origins of dysbiotic microbiota. [A] Schematic diagram of the filial generation of littermate genotype-based separation [LGS] groups. Hemizygote-bred mouse pups of three genotypes [WT/WT], [Tg/WT], and [Tg/Tg], were nursed by WT dams during the neonatal period, and then caged separately according to genotypes after weaning. The time-series changes in epithelial and faecal microbiota were monitored in the LGS groups at the ages of 3, 6, and 10 weeks [w]. [B] Colonic epithelial samples were collected pre-weaning at the age of [a] 3 w, and post-weaning at the ages of [b] 6 w and [c] 10 w for microbiota comparison. Clustering of the epithelial microbiota was observed at the age of 3 w across the mouse genotypes of LGS[WT/WT] [red], LGS[Tg/WT] [blue], and LGS[Tg/Tg] [green]. Distinct compositions of epithelial microbiota between LGS[Tg/Tg] and LGS[WT/WT] groups were noted at 6 w and 10 w. Each dot represents one mouse. *N* = 5/group. [C] Clustering of the faecal microbiota among LGS groups was observed at the ages of [a] 3 w and [b] 6 w, but not at [c] 10 w. The faecal microbiota of LGS[Tg/Tg] was not distinguishable from that of LGS[WT/WT] until 10 w of age. Each dot represents one mouse. *N* = 5/group. [D] Higher IEB counts were noted in the pre-weaning phase at 3 w compared with those in adulthood at 6, 8, and 10 w for all

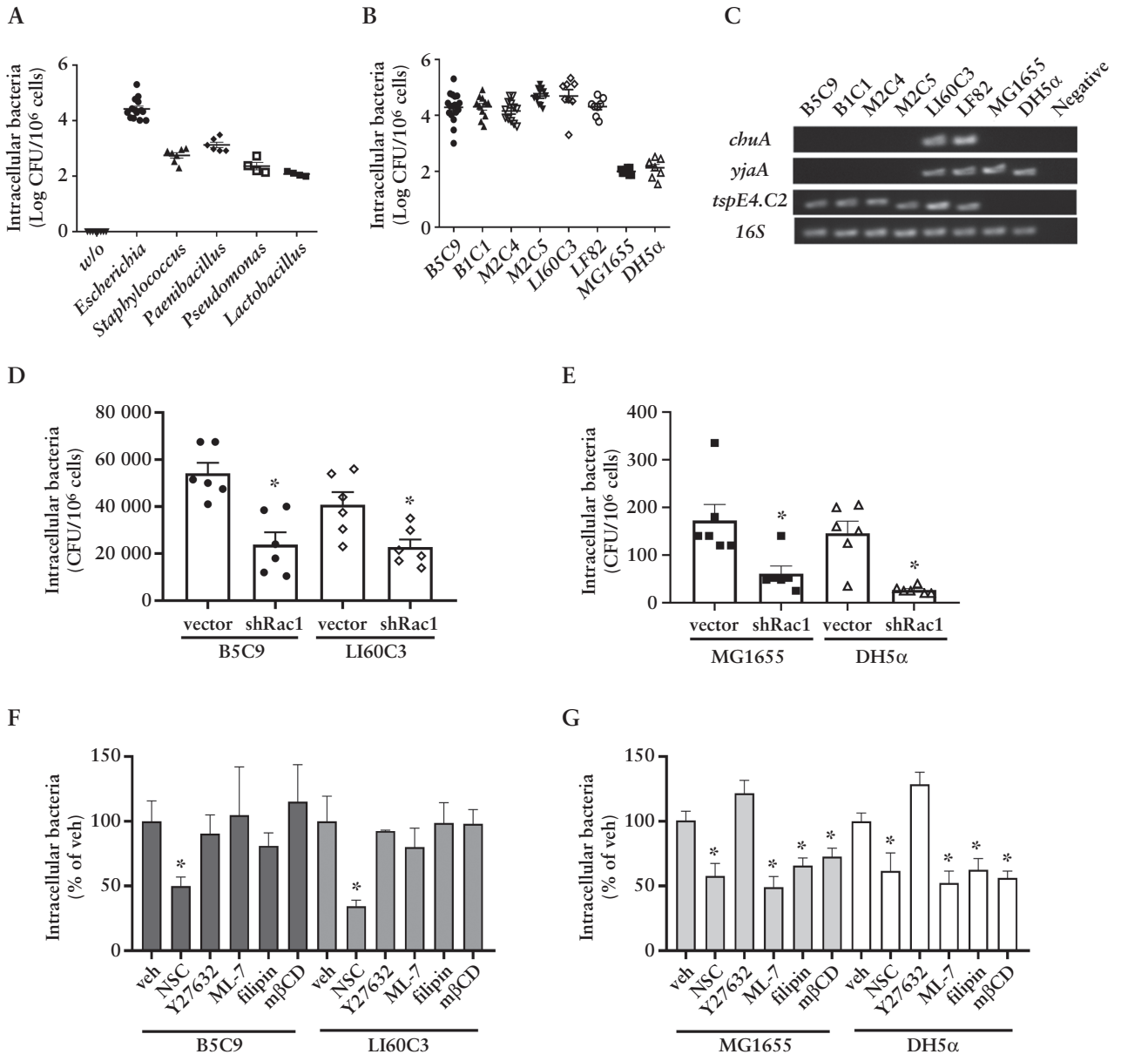

Figure 4. Mouse-isolated intraepithelial *E. coli* showed invasive behaviour in human epithelial cultures in a RAC1-dependent but MLCK-independent manner. Mouse-isolated bacteria were exposed to Caco-2 epithelial cell cultures *in vitro* at equal multiplicity-of-infection [MOI] values for comparison of IEB counts. [A] Higher IEB counts were observed for *Escherichia* than for other bacterial genera isolated from mouse colonocytes. $N = 6$/group.$p < 0.05$ vs. w/o. [B] The IEB counts of mouse-isolated *E. coli* [B5C9, B1C1, M2C4, M2C5, and LI60C3] were comparable to a Crohn's adherent-invasive *E. coli* LF82 and were 1000-fold higher than those of laboratory K-12 strains [MG1655 and DH5α]. The data suggested invasive modes for B5C9 and LI60C3. [C] Phylogroup profiling of *E. coli* using Clermont's triplex PCR assay based on the presence or absence of three genes, namely, *chuA*, *yjaA*, and *tspE4.C2*. The results showed *E. coli* belonging to phylogroup B1 [strains B5C9, B1C1, M2C4, and M2C5], phylogroup B2 [strains LI60C3 and LF82], and phylogroup A [strains MG1655 and DH5α]. Negative controls did not contain bacterial samples. [D and E] Gene silencing of actin-associated *RAC1* reduced the IEB counts of invasive strains [B5C9 and LI60C3] and noninvasive strains [MG1655 and DH5α]. [F] The IEB counts of B5C9 and LI60C3 were reduced by NSC23766 [NSC, a specific Rac1 inhibitor] but not by ML-7 [an MLCK inhibitor], Y27632 [a ROCK inhibitor], or cholesterol-sequestering agents such as filipin and mβCD. [G] The IEB counts of MG1655 and DH5α were decreased by all of the inhibitors, except Y27632. $N = 6$/group. $^{*}p < 0.05$ vs. w/o. IEB, intraepithelial bacteria; PCR, polymerase chain reaction.

LGS groups. The IEB counts of adult LGS[Tg/Tg] were higher than those of adult LGS[WT/WT]. $N = 10$/group. $^{*}p < 0.05$ vs. age-matched LGS[WT/WT]. $^{\#}p < 0.05$ vs. 3 w. [E] No difference in occludin levels and dextran flux in colonic tissues among the LGS groups. $N = 10$/group. [F] The Shannon diversity of the epithelial microbiota [left] and faecal microbiota [right] in the LGS groups at 3, 6, and 10 w. $N = 5$/group. $^{*}p < 0.05$ vs. age-matched LGS[WT/WT]. The Shannon index in epithelial microbiota of LGS[Tg/Tg] was lower than that of LGS[WT/WT] at an early age. Higher Shannon index was observed in the epithelial than in the faecal microbiota for all LGS groups, but the statistical labels were omitted for data clarification. [G] Heatmap of the epithelial microbiota [left] and faecal microbiota [right] among the LGS groups at 3 w. Representative data of two out of five samples are shown for clarification. [H] Ratio of the relative abundance of epithelial bacteria [left] and faecal bacteria [right] by comparing the LGS[Tg/Tg] and LGS[WT/WT] groups. A 5-fold higher abundance of *Escherichia* was noted in the epithelial compartment of LGS[Tg/Tg]. A 2-fold higher abundance of *Escherichia* was noted in the faecal samples of LGS[Tg/Tg]. $N = 5$/group. [I] Negligible levels of intestinal MPO activity in the untreated LGS groups at steady state. [J and K] Intestinal MPO activity of the LGS groups after treatment with colitogenic agents, DSS and TNBS. $N = 6$–10/group. $^{*}p < 0.05$ vs. age-matched LGS[WT/WT]. WT, wild type; MPO, myeloperoxidase; DSS, dextran sodium sulphate; TNBS, trinitrobenzene sulphonic acid; IEB, intraepithelial bacteria.

Table 1. Antibiogram of *Escherichia coli* strains

Strain	B1C1		B5C9		M2C4		M2C5		LI60C3		LF82		MG1655		DH5α	
Antimicrobial agent	MIC [μg/ml]	Result	MIC [μg/ml]	Result	MIC [μg/ml]	Result	MIC [μg/ml]	Result	MIC [μg/ml]	Result	MIC [μg/ml]	Result	MIC [μg/ml]	Result	MIC [μg/ml]	Result
Amikacin	≤2	S	≤2	S	≤2	S	≤2	S	≤2	S	8	S	≤2	S	≤2	S
Ampicillin	≥32	R	≥32	R	≥32	R	≥32	R	≥32	R	≥32	R	≤2	S	≤2	S
Cefazolin	32	R	≥64	R	≥64	R	≥64	R	≥64	R	≥64	R	≤4	S	≤4	S
Cefepime	≤1	S	≤1	S	≤1	S	≤1	S	≤1	S	≤1	S	≤1	S	≤1	S
Cefmatazole	32	I	32	I	32	I	32	I	32	I	32	I	≤1	S	≤1	S
Cefotaxime	≤1	S	≤1	S	≤1	S	≤1	S	≤1	S	4	R	≤1	S	≤1	S
Ceftazidime	≤1	S	≤1	S	≤1	S	≤1	S	≤1	S	16	R	≤1	S	≤1	S
Ciprofloxacin	≤0.25	S	≤0.25	S	≤0.25	S	≤0.25	S	≤0.25	S	≤0.25	S	≤0.25	S	≤0.25	S
Colistin	≤0.5	I	≤0.5	I	≤0.5	I	≤0.5	I	≤0.5	I	≤0.5	I	≤0.5	I	≤0.5	I
Ertapenem	≤0.5	S	≤0.5	S	≤0.5	S	≤0.5	S	≤0.5	S	≤0.5	S	≤0.5	S	≤0.5	S
Gentamicin	≤1	S	≤1	S	≤1	S	≤1	S	≤1	S	≤1	S	≤1	S	≤1	S
Imipenem	≤0.25	S	≤0.25	S	≤0.25	S	≤0.25	S	≤0.25	S	0.5	S	≤0.25	S	≤0.25	S
Levofloxacin	≤0.12	S	≤0.12	S	≤0.12	S	≤0.12	S	≤0.12	S	≤0.12	S	≤0.12	S	≤0.12	S
Meropenem	≤0.25	S	≤0.25	S	≤0.25	S	≤0.25	S	≤0.25	S	≤0.25	S	≤0.25	S	≤0.25	S
Piperacillin	8	S	8	S	8	S	8	S	8	S	64	I	≤4	S	≤4	S
Tigecycline	≤0.5	S	≤0.5	S	≤0.5	S	≤0.5	S	≤0.5	S	≤0.5	S	≤0.5	S	≤0.5	S
Trimethoprim	≤20	S	≤20	S	≤20	S	≤20	S	≤20	S	≤20	S	≤20	S	≤20	S

MIC, minimum inhibitory concentration; S, sensitive; R, resistant; I, intermediate.

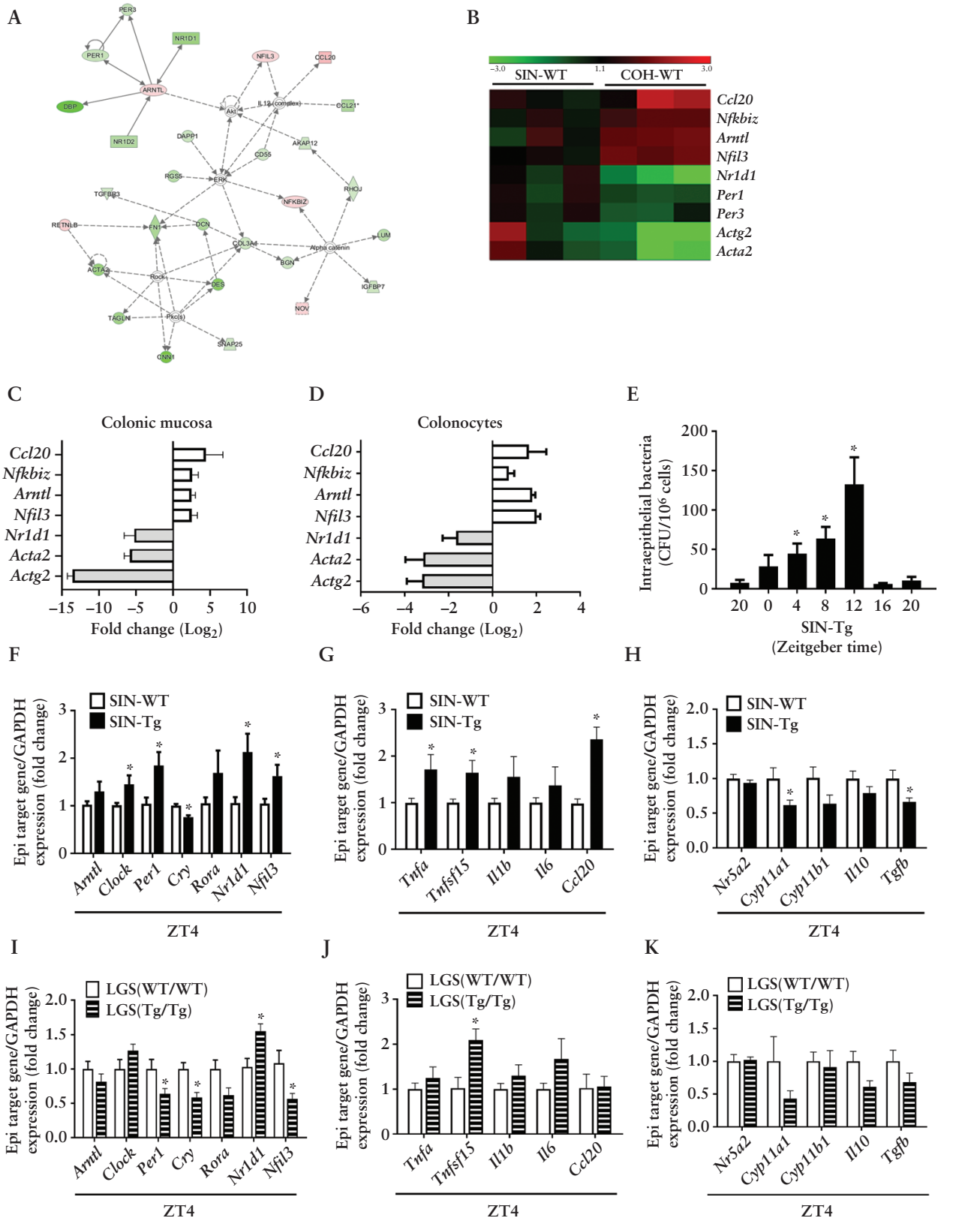

Figure 5. Epithelial circadian disruption was observed in mice harbouring IEB. Gene array was performed to explore alternative host responses to IEB involved in the exacerbation of colitis. Transcriptome profiles in SIN-WT and COH-WT mice were evaluated to avoid confounding factors of excessive MLCK activation in the MLCK-Tg mice. The SIN-WT and COH-WT mice were both of a WT background, but the latter harboured IEB. [A] Circadian rhythm was the most cohesive network for differences between SIN-WT and COH-WT mice. Red colour indicates the gene expressions higher in COH-WT mice, whereas green colour indicates those higher in SIN-WT mice. Arrows in solid line were direct connection and those in dotted line were indirect connection. [B] Heatmap analysis shows altered mucosal transcriptomes in COH-WT mice, including cytokine, circadian, and cytoskeletal remodelling. *N* = 5/group. [C and D] qPCR analysis of gene expression in colonic mucosa and colonocytes from SIN-WT and COH-WT mice. [E] The

of particular IEB strains due to epithelial MLCK activation, such as *Escherichia*, caused faecal microbiota conversion from eubiosis to dysbiosis.

3.4. Classification of invasive and noninvasive microbes among the IEB population

Human Caco-2 intestinal epithelial cultures were then challenged with mouse-isolated IEB strains, and the intracellular counts were determined using a gentamicin resistance assay. Higher intracellular counts were observed when challenged with mouse isolates of *Escherichia* compared with *Staphylococcus, Paenibacillus, Pseudomonas,* or *Lactobacillus* [Figure 4A]. All mouse-isolated *E. coli* strains [ie, B5C9, B1C1, M2C4, and M2C5] showed high IEB counts [Figure 4B] and displayed gentamicin susceptibility [Table 1]. Other *E. coli* strains, including invasive LI60C3 obtained from DSS-treated mice,[33] Crohn's disease adherent-invasive LF82,[19] and laboratory noninvasive K-12 strains [MG1655 and DH5α], were also tested. The IEB counts of mouse-isolated *E. coli* were comparable to LF82, and were ~1000-fold greater than laboratory K-12 strains [Figure 4B]. The strains B5C9, B1C1, M2C4, and M2C5 were classified as phylogroup B1; LI60C3 and LF82 were classified as phylogroup B2; and MG1655 and DH5α were classified as phylogroup A based on the presence of *chuA*, *yjaA*, and *tspE4.C2* genes [Figure 4C].

3.5. Bacterial invasion was dependent on Rac1 but not MLCK in epithelial cells

Previous studies have shown that Rho family GTPases, including Rac1 and Rho-associated kinase [ROCK], are critical regulators of actin structure and apical bacterial entry.[43] On the other hand, we have shown that MLCK activates brush border fanning to facilitate caveolar endocytosis of noninvasive bacteria.[10,11] *E. coli* strains B5C9 and LI60C3 were used as representative invasive bacteria of phylogroups B1 and B2, respectively, and compared with phylogroup A laboratory K-12 *E. coli*.

Gene silencing of *RAC1* reduced the IEB counts of B5C9, LI60C3, MG1655, and DH5α in Caco-2 cells [Figure 4D and E], suggesting that Rac1 was involved in epithelial entry for invasive and noninvasive strains. Consistent with this, the IEB counts of B5C9 and LI60C3 were also reduced by the Rac1 inhibitor NSC23766 but not by the MLCK inhibitor ML-7 or the cholesterol-sequestering agents filipin or mβCD [Figure 4F]. In contrast, numbers of MG1655 and DH5α bacteria in Caco-2 cells were reduced by pretreatment with NSC23766, ML-7, filipin, and mβCD [Figure 4G]. Based on the IEB counts and dependence on epithelial MLCK activation for endocytosis, MG1655 and DH5α strains can be considered noninvasive whereas B5C9 and LI60C3 strains are invasive bacteria.

3.6. Invasive bacteria evoked circadian disruption in the gut mucosa

An unbiased gene microarray approach was used to explore host responses to IEB that could be involved in colitis exacerbation within MLCK-Tg mice and WT mice colonised with MLCK-Tg microbiota. Colonic mucosal transcriptome profiles of SIN-WT and COH-WT mice, which were co-housed with MLCK-Tg mice and had IEB, were analysed to avoid potential confounding factors of MLCK activation in MLCK-Tg mice. Ingenuity pathway analysis [IPA] revealed the top differences to be within agranulocyte adhesion and diapedesis, circadian rhythm, and actin cytoskeletal signalling pathways, all of which were increased in COH-WT mice relative to SIN-WT mice. Gene network construction identified key modules and candidate hub genes in circadian rhythm as the most cohesive network to explain activation of these pathways in colonic mucosa of COH-WT mice [Figure 5A]. We anticipated IEB might induce leukocyte infiltration and cytoskeletal rearrangement but did not expect the pronounced association with circadian rhythm disruption.

Circadian rhythm is coordinated by an interlocking 24-h clock system regulated by daylight through input stimuli from the optic nerve of the eye.[44] Circadian regulation of gene transcription also occurs within the gastrointestinal tract, where colonic epithelial cells express high levels of circadian rhythm-related proteins.[45,46] Microarray analyses revealed increased expression of the circadian rhythm genes *Arntl* and *Nfil3* and reduced expression of *Nr1d1*, *Per1*, and *Per3* in colonic mucosa of COH-WT, relative to SIN-WT, mice [Figure 5B]. Increased *Arntl* and *Nfil3* and decreased *Nr1d1* expression were confirmed by qPCR of colonic mucosa and purified colonocytes of COH-WT, relative to SIN-WT, mice [Figure 5C and D].

To identify the appropriate time for analysis of circadian effects, IEB abundance of conventionally raised MLCK-Tg mice in SIN conditions were determined. Numbers of IEB were lowest at Zeitgeber time [ZT] 20 [2 am, nadir] and highest at ZT12 [6 pm, peak] [Figure 5E]. IEB numbers increased during the daylight phase from ZT0 to ZT4 [6 am to 10 am] [Figure 5E]. Circadian gene expression was, therefore, assessed in mucosal samples collected at ZT4, the time at which bacterial entry increase were most prominent. Expression of *Nr1d1*, *Nfil3*, *Clock*, and *Per1* were increased in epithelial cells of SIN-Tg mice relative to SIN-WT mice at ZT4 [Figure 5F]. Cytokine profiles identified increased expression of proinflammatory genes *Tnfa* and *Tnfsf15* levels and decreased anti-inflammatory *Tgfb* and glucocorticoid enzyme *Cyp11a1* expression in cells at ZT4 [Figure 5G and H]. Altered expression of circadian rhythm genes *Nr1d1* and *Nfil3* was also observed in mucosal samples from LGS[Tg/Tg] mice relative to LGS[WT/WT] mice at ZT4 [Figure 5I]. *Tnfsf15*

IEB counts at different Zeitgeber time [ZT]. The intracellular bacterial numbers increased at ZT4 [10:00] and peaked at ZT12 [18:00] which correlated with the daylight phase. Low IEB counts were observed at ZT20 [2:00] which correlated with the dark phase and wake period for nocturnal animals. The ZT4 signifies the start of bacterial entry and were chosen as the time point for assessment of circadian and cytokine gene expression. $N = 5$/group. *$p \leq 0.05$ vs. ZT20. Experiments repeated twice. [F] Altered circadian expression in colonocytes of SIN-Tg mice compared with SIN-WT mice at ZT4. The colonocytes were collected from 8-week old mice at a steady state. [G] Increased proinflammatory cytokine levels in colonocytes of SIN-Tg mice compared with SIN-WT mice at ZT4. [H] Decreased glucocorticoid-related gene and anti-inflammatory cytokine expression in the colonocytes of SIN-Tg mice compared with SIN-WT mice at ZT4. $N = 5$/group. *$p \leq 0.05$ vs. SIN-WT. [I] Altered circadian expression in the colonocytes of LGS[WT/WT] and LGS[Tg/Tg] at ZT4. The colonocytes were collected from 10-week old LGS groups at a steady state. [J] Increased proinflammatory cytokine levels of LGS[Tg/Tg] mice compared with LGS[WT/WT] mice at ZT4. [K] Decreased glucocorticoid-related gene and anti-inflammatory cytokine expression in the colonocytes of LGS[Tg/Tg] compared with LGS[WT/WT] at ZT4. $N = 5$/group. *$p \leq 0.05$ vs. LGS[WT/WT]. WT, wild type; IEB, intraepithelial bacteria; qPCR, quantitative polymerase chain reaction; LGS, littermate genotype-based separation.

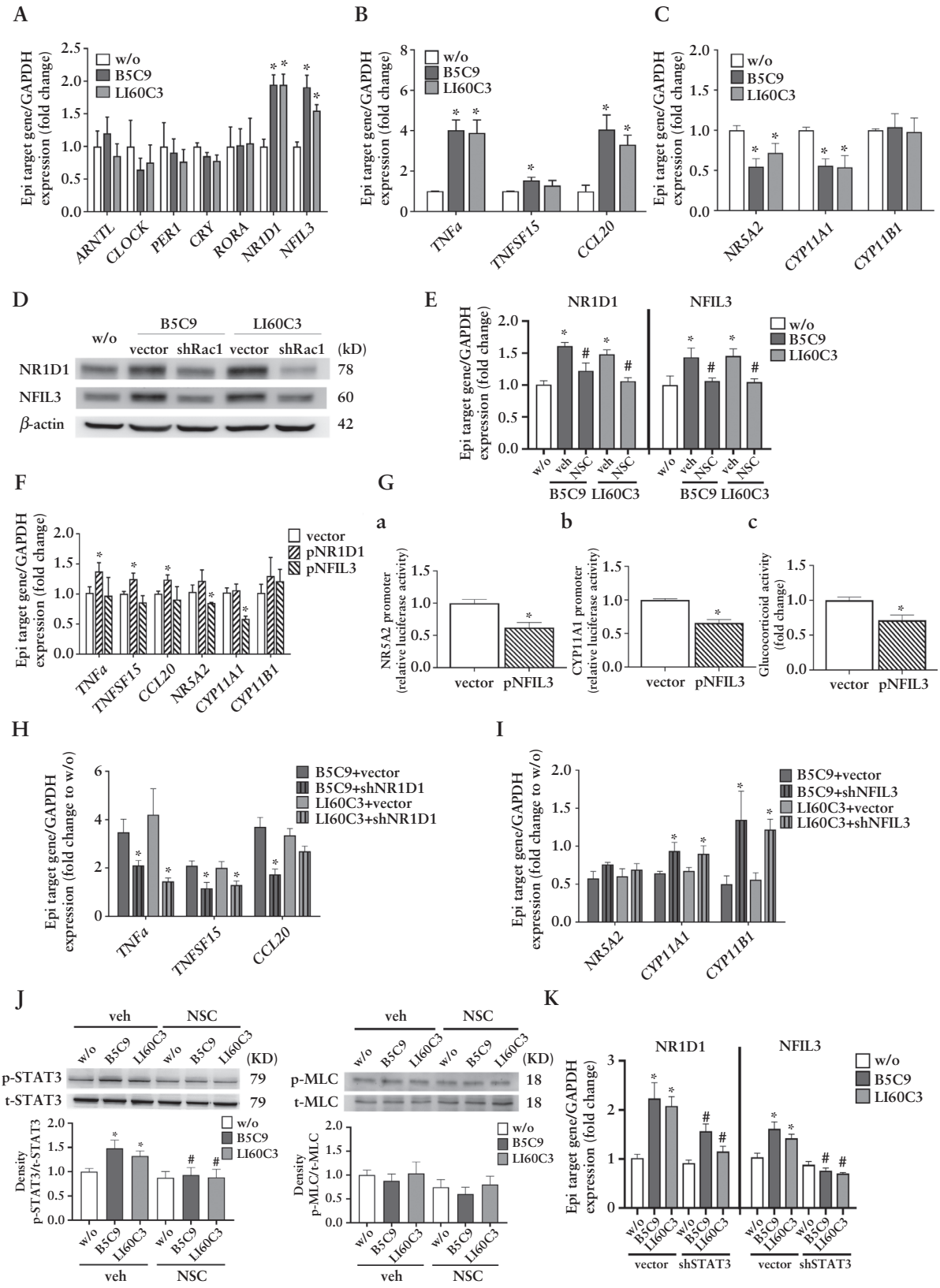

Figure 6. Bacterial invasion triggered epithelial circadian disruption and proinflammatory responses via Rac1/STAT3 signalling. Bacteria-epithelial co-cultures were assessed for IEB-induced circadian changes. [A] Upregulated circadian *NR1D1* and *NFIL3* gene expression was observed in Caco-2 cells 1 h after exposure to invasive bacteria. $N = 6$/group. $^{*}p < 0.05$ vs. w/o. [B and C] Exposure to invasive bacteria increased proinflammatory cytokines and decreased glucocorticoid-related enzyme expression. [D] Bacteria-induced circadian NR1D1 and NFIL3 protein upregulation was prevented by *RAC1* gene silencing. [E] Pre-treatment with NSC23766 [NSC] attenuated bacteria-induced epithelial circadian changes. $^{*}p < 0.05$ vs. w/o. $^{\#}p < 0.05$ vs. vehicle. [F] Overexpressing *NR1D1* increased proinflammatory cytokine while overexpressing *NFIL3* decreased glucocorticoid-related expression in Caco-2 cells in the absence of bacteria. [G] Overexpressing NFIL3 induced [a] *NR5A2* and [b] *CYP11A1* promoter activities and

expression was increased and there was a trend towards reduced *Cyp11a1* expression in colonocytes of LGS[Tg/Tg] mice relative to LGS[WT/WT] mice at ZT4 [Figure 5J and K]. These data suggest that IEB-induced epithelial circadian disruption is an early event the precedes overt inflammation.

3.7. Invasive bacteria trigger NR1D1-dependent proinflammatory cytokine upregulation and NFIL3-mediated suppression of glucocorticoid synthesis

Circadian-dependent transcriptional activity on cytokine production was evaluated in the bacteria-epithelial cocultures. Challenge with invasive B5C9 and LI60C3 elevated the *NR1D1* and *NFIL3* levels in Caco-2 cells [Figure 6A]. Increases in proinflammatory *TNFα*, *TNFSF15*, and *CCL20* levels [Figure 6B] were accompanied by a decrease in the glucocorticoid-related *NR5A2* and *CYP11A1* gene expression [Figure 6C] after bacterial exposure. Gene silencing of *RAC1* and pretreatment with NSC23766 [a specific Rac1 inhibitor] prevented the bacteria-induced elevation of NR1D1 and NFIL3 protein and mRNA levels [Figure 6D and E].

Circadian regulation of cytokine production was initially evaluated by overexpressing *NR1D1* in Caco-2 cells, which led to increased *TNFα*, *TNFSF15*, and *CCL20* expression but no change in glucocorticoid-related gene expression [Figure 6F]. Conversely, *NFIL3* overexpression reduced *NR5A2* and *CYP11A1* expression but did not affect proinflammatory cytokine expression [Figure 6F]. A luciferase reporter assay confirmed NFIL3-mediated repression of *NR5A2* and *CYP11A1* promoter activity [Figure 6G]. Further, *NR1D1* knockdown attenuated bacteria-induced upregulation of proinflammatory cytokines [Figure 6H], whereas *NFIL3* knockdown prevented bacteria-induced suppression of glucocorticoid-related genes [Figure 6I].

As signal transducer and activator of transcription factor 3 [STAT3] binds directly to Rac1,[47] we examined STAT3 phosphorylation downstream of bacterial invasion-induced Rac1 activation. STAT3 phosphorylation induced by invasive bacteria was inhibited by pretreatment with NSC23766 [Figure 6J]. *STAT3* knockdown also attenuated bacteria-induced *NR1D1* and *NFIL3* expression [Figure 6K]. As a whole, these data indicate that bacterial invasion disrupts epithelial circadian rhythm via a Rac1/STAT3-dependent process.

3.8. Colitogenic ability of invasive bacteria was ablated by Rac1 inhibition in mice

To investigate the colitogenic potential of invasive *E. coli in vivo*, WT mice were gavaged with B5C9, LI60C3, DH5α, or vehicle [PBS]. B5C9 or LI60C3 reduced body weight relative to that of mice that received DH5α or PBS [Figures 7A]. Further, mice inoculated with B5C9 or LI60C3 showed increased bacterial colonisation and exacerbated colitis relative to those with DH5α or PBS [Figures 7B and 7C]. Finally, treatment with the Rac1 inhibitor NSC23766 reduced bacterial colonisation and attenuated colitis severity in B5C9-infected mice [Figure 7D and E]. NSC23766 also decreased epithelial expression of *Nr1d1*, *Nfil3*, *Tnfa*, and *Ccl20*, and increased expression of glucocorticoid-related *Cyp11a1* genes in colonocytes of B5C9-infected mice [Figure 7F]. The reduction of bacterial colonisation by NSC23766 was also accompanied by attenuated colitis severity and decreased *Nr1d1* and *Ccl20* levels in the epithelial cells of LI60C3-infected mice [Figure 7G-I].

4. Discussion

Our findings provide evidence of a mechanism by which barrier defects affect microbial dysbiosis and exacerbate colitis. Epithelial MLCK activation enhanced endocytosis of commensal bacteria, evoked conversion to invasive pathobionts, and enhanced development of a colitogenic microbiota. Moreover, invasive bacteria disrupted epithelial circadian rhythm via a Rac1/STAT3-dependent, MLCK-independent, process that led to upregulation of proinflammatory cytokines and downregulation of anti-inflammatory glucocorticoid expression [Figure 7J]. The data further pinpoint invasive pathobionts as a trigger for circadian dysrhythmia that shifts the balance of colonocyte proinflammatory responses to exacerbate colitis.

Faecal and mucosal microbial changes have been documented in treatment-naïve IBD patients. Key findings include *Enterobacteriaceae* enrichment and reduced abundance of core commensals, including *Bacteroidiales* and *Clostridiales*, in ileal and colonic resection specimens from newly diagnosed pediatric CD and UC patients[6,7] as well as a decrease in butyrate-producing bacteria, such as *Faecalibacterium*, *Ruminococcus*, and *Roseburia*, and immune-regulatory species, such as *Akkermansia*.[6] To investigate the origins of dysbiosis in MLCK-Tg mice, we developed a novel breeding strategy using WT nursing dams and littermate genotype-based separation to monitor the conversion of eubiotic commensals to dysbiotic pathobionts longitudinally. This model revealed distinct microbiota between MLCK-Tg and WT littermates after weaning. The divergence of microbial populations correlated with increased colitis severity and is consistent with a previous report showing segregation of faecal microbiota between MLCK-Tg and WT littermates born to WT dams.[48]

Among IEB, *Escherichia* were enriched in MLCK-Tg mice at weaning. These and other data suggest that expansion of intraepithelial *Escherichia* drives dysbiosis of faecal bacteria. Our LGS study also identified epithelial microbiota with greater alpha-diversity than faecal microbiota, likely due to the unique biology of neonatal enterocytes and the reduced barrier function, observed in both rodent pups and human infants, and the dynamic shifts in neonatal intestinal microbial ecology.[41,42] Preweaning epithelial microbiota might, therefore, serve as a reservoir for the faecal microbiome. Differences between the epithelial and faecal microbiota for each mouse were observed at an early age and persisted to adulthood, indicating that oxygen levels and dietary elements contributed to the configuration of distinct microbial compositions at adjacent sites. Considering that normal

increased [c] glucocorticoid activity. $N = 6$/group. *$p \leq 0.05$ vs. vector. [H] Knockdown of *NR1D1* reduced the bacteria-upregulated proinflammatory cytokines. [I] Knockdown of *NFIL3* reversed the bacteria-induced glucocorticoid suppression. *$p < 0.05$ vs. vector. [J] Invasive bacteria induced epithelial STAT3 phosphorylation, which was prevented by NSC23766 treatment. The NSC treatment did not cause changes in MLCK phosphorylation. Western blots shown were representative of two experiments. *$p \leq 0.05$ vs. w/o. #$p \leq 0.05$ vs. vehicle. [K] Bacteria-induced circadian *NR1D1* and *NFIL3* gene expression was decreased by *STAT3* silencing. *$p \leq 0.05$ vs. w/o. #$p \leq 0.05$ vs. vector. IEB, intraepithelial bacteria.

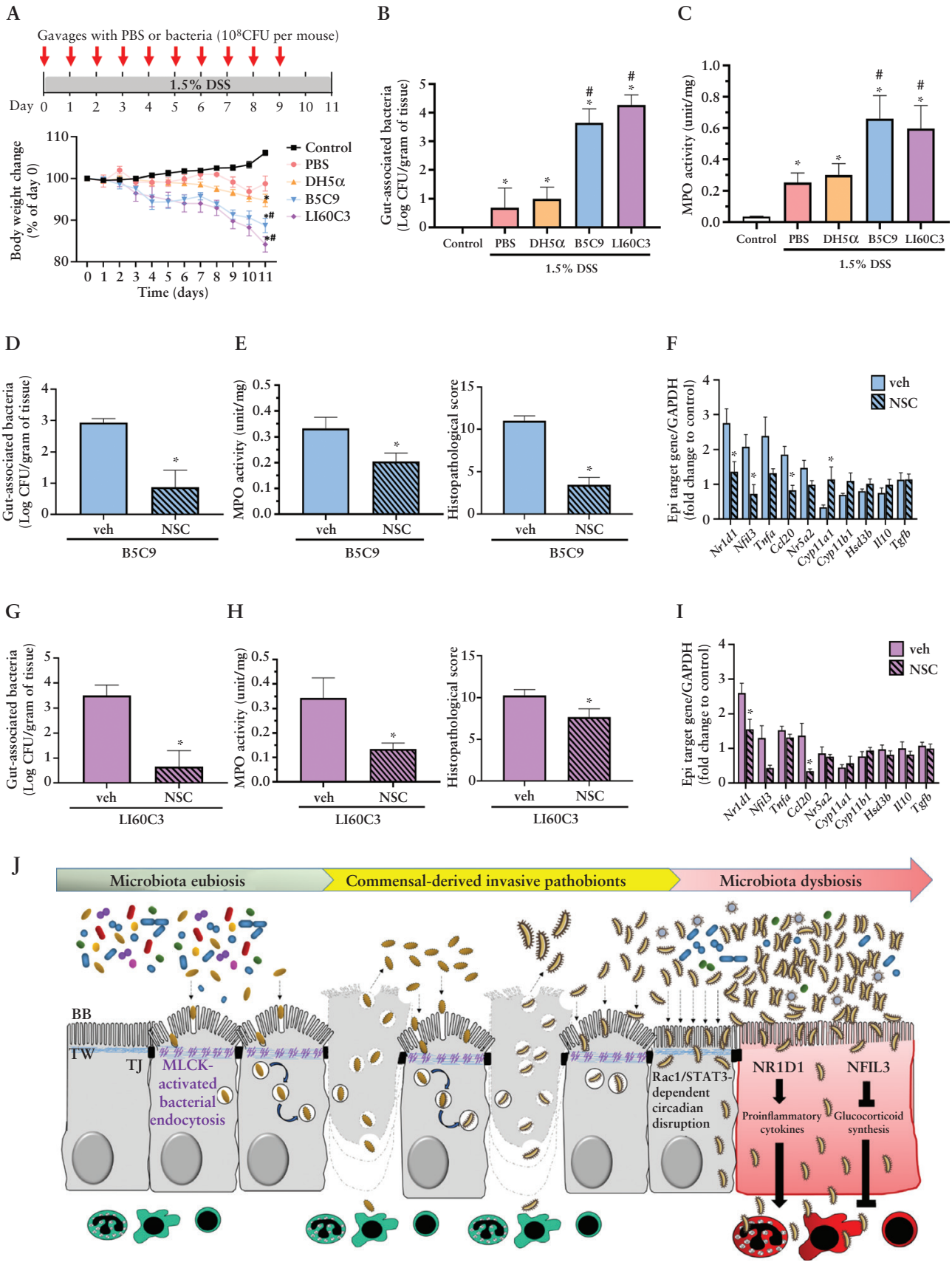

Figure 7. Epithelial circadian-driven inflammation in response to pathobiont invasion was ablated by Rac1 inhibition in mouse models. [A] Time line of bacterial infection in mice to investigate the colitogenic ability of *E. coli*. The WT mice were drinking DSS water and gavaged with vehicle [PBS] or bacteria [DH5α, B5C9, and LI60C3]. Control mice drank normal water without bacterial challenge. Daily body weight change is shown. $N = 10$/group. $^{*}p < 0.05$ vs. control. $^{\#}p < 0.05$ vs. PBS. [B and C] Higher gut-associated bacterial counts and MPO activity in mice inoculated with B5C9 and LI60C3 compared with the PBS or DH5α group. [D] Mice were injected with a specific Rac1 inhibitor NSC23766 [NSC] prior to bacterial inoculation. NSC

colonocytes are highly oxygenated compared with the low-oxygen lumen environment, inhabitants that are facultative anaerobes [eg, *Escherichia*, *Staphylococcus*, *Paenibacillus*, and *Pseudomonas*] and oxygen-tolerant anaerobes [eg, *Lactobacillus*] have more advantages over obligate anaerobes for intracellular survival. Among anaerobes suitable for intraepithelial survival, we and others have identified *E. coli* with pathobiont potential in IBD and cancers.

We found that distinct modes of bacterial entry correlated with epithelial circadian disruption. Rac1/STAT3-dependent microbial invasion triggered cytokine upregulation via disruption of epithelial circadian rhythm, whereas MLCK activation enhanced caveolar bacterial endocytosis that did not affect circadian rhythm. Previous studies have shown that invasive pathogens[49,50] and mitochondrial dysfunction[51–54] trigger transcytosis of noninvasive bacteria, suggesting that commensal endocytosis and invasive pathobionts may be mutually enhanced via a positive-feedback loop that drives long-term dysbiosis. Consistent with this, Rac1 inhibition prevented entry of both invasive and noninvasive bacteria *in vitro*, attenuated epithelial circadian disruption, and reduced colitis severity. This could, potentially, correlate with a report that Rac1 inhibition improves barrier function in models of necrotsiing enterocolitis models and prevents *in vitro* internalisation of adherent-invasive *E. coli*.[55,56] It is, therefore, plausible that Rac1 is critically involved in colitis pathogenesis by modulating epithelial cytoskeletal dynamics and aggravating pathobiont conversion and dysbiosis.

The gene array data led to our discovery that the microbiota-circadian axis contributes to inflammation. Consistent with this, altered circadian rhythms have been reported in IBD patient biopsies,[57] and epithelium-specific BMAL1/RORα deficiency promoted colitis and proinflammatory signalling in mice and organoid models, respectively.[58,59] Invasive pathobionts, which are internalised via a Rac1-dependent process, disrupted the epithelial circadian clock to control the balance of proinflammatory responses, whereas commensal bacteria, which are endocytosed via an MLCK- and caveolin-dependent process, do not. Consistent with this, disruption of diet-induced diurnal microbiome fluctuations is associated with increased enteritis susceptibility[60] and risk of metabolic syndrome.[61,62] Previous studies also demonstrated circadian variation in microbiota composition and bacterial adherence which influences host transcriptome oscillation.[63] We found that intraepithelial bacterial counts begin to rise at ZT4 [10:00] and peak at ZT12 [18:00], suggesting that bacterial invasive capacity increases during the daylight phase, which is the sleep period for nocturnal animals. The peak was followed by a sharp decline in IEB numbers from ZT16 [22:00] until ZT20 [2:00], the awake period for food ingestion in mice. The results suggest that food intake and associated peristalsis and defaecation may, in part, account for changes in the microbiota and IEB numbers.

In conclusion, MLCK-dependent barrier defects were a cause of microbial dysbiosis and pathobiont emergence that, in turn, exacerbated colitis by disrupting the epithelial circadian clock and promoting the epithelial proinflammatory responses. These data reveal a previously unrecognised mechanism by which invasive pathobionts trigger epithelial circadian rhythm-dependent inflammation. This new insight may enable development of barrier-protective, bacterium-targeted precision medicine therapies.

Availability of data and material: Data is available upon request the gene array and bacterial 16S rDNA sequencing data were submitted to the GEO database [GSE212393, GSE212394, GSE212834, GSE212822, GSE212813].

Funding

This study was funded by the Ministry of Science and Technology, Taiwan [MOST 110-2320-B-002-011-MY3, MOST 111-2811-B-002-009, and MOST 111-2811-B-002-061], National Health Research Institutes, Taiwan [NHRI-EX111-11108BI, NHRI-EX112-11108BI, NHRI-EX113-11108BI], and National Taiwan University Core Consortium projects, Taiwan [NTU-CC-112L895002] to LCY, and National Institutes of Health, United States [R01DK061931, R01DK068271] to JRT.

Conflict of Interest

The authors declare that they have no competing interests.

Author contributions

Guarantor of integrity of the entire study, LCY; study concepts and design: YCP, LCY; data acquisition: YCP, YHL; data analysis/interpretation: YCP, YHL; statistical analysis: YCP, YHL; material and technical support: JRT; obtained funding: YCP, JRT, LCY; manuscript drafting or revision for important intellectual content, literature research, manuscript editing, and manuscript final version approval: all authors.

Acknowledgements

We thank the staff of the imaging and sequencing facility at the First Research Core, Animal Center, Medical Microbiota Core, and Genomic Core in NTUCM and the Department of Laboratory Medicine in NTUH for their technical assistance. This article was subsidised for English editing by National Taiwan University under the Excellence Improvement Program for Doctoral Students [grant number 108-2926-I-002-002-MY4], sponsored by the Ministry of Science and Technology, Taiwan.

treatment decreased gut-associated bacterial counts in the B5C9-infected mice. [E and F] NSC treatment reduced colitis and circadian disruption in B5C9-infected mice. *$P < 0.05$ vs. vehicle. [G] NSC treatment decreased the gut-associated bacterial counts in LI60C3-infected mice. [H and I] NSC treatment reduced colitis and circadian disruption in LI60C3-infected mice. [J] Proposed schema of the relationship between epithelial barrier defects and microbiota dysbiosis for predisposition to colitis. Eubiotic commensals interfacing epithelial cells with intact brush borders [BB], terminal web [TW], and tight junctions [TJ] are in juxtaposition to immune cells in a healthy status. Epithelial MLCK-activated BB fanning facilitated passive endocytosis of commensal bacteria. The internalised bacteria that survived against intracellular stress were released into the luminal space by epithelial shedding. Repeated exposure of bacteria to intracellular stress led to their conversion from eubiotic commensals to invasive pathobionts, forming a dysbiotic microbiota. The invasive pathobionts triggered Rac1/STAT3-dependent epithelial circadian disruption, including NR1D1-upregulated proinflammatory cytokines and NFIL3-downregulated glucocorticoid synthesis. The pathobiont-driven epithelial proinflammatory response initiates colitis development in the host. WT, wild type; MPO, myeloperoxidase; DSS, dextran sodium sulphate; PBS, phosphate-buffered saline.

Supplementary Data

Supplementary data are available at *ECCO-JCC* online.

References

1. Arnott ID, Kingstone K, Ghosh S. Abnormal intestinal permeability predicts relapse in inactive Crohn disease. *Scand J Gastroenterol* 2000;**35**:1163–9.
2. D'Inca R, Di Leo V, Corrao G, *et al*. Intestinal permeability test as a predictor of clinical course in Crohn's disease. *Am J Gastroenterol* 1999;**94**:2956–60.
3. Turpin W, Lee SH, Raygoza Garay JA, *et al*. Increased intestinal permeability is associated with later development of Crohn's disease. *Gastroenterology* 2020;**159**:2092–100 e5.
4. Swidsinski A, Weber J, Loening-Baucke V, Hale LP, Lochs H. Spatial organization and composition of the mucosal flora in patients with inflammatory bowel disease. *J Clin Microbiol* 2005;**43**:3380–9.
5. Kleessen B, Kroesen AJ, Buhr HJ, Blaut M. Mucosal and invading bacteria in patients with inflammatory bowel disease compared with controls. *Scand J Gastroenterol* 2002;**37**:1034–41.
6. Putignani L, Oliva S, Isoldi S, *et al*. Fecal and mucosal microbiota profiling in pediatric inflammatory bowel diseases. *Eur J Gastroenterol Hepatol* 2021;**33**:1376–86.
7. Gevers D, Kugathasan S, Denson LA, *et al*. The treatment-naive microbiome in new-onset Crohn's disease. *Cell Host Microbe* 2014;**15**:382–92.
8. Lee Y, Sugihara K, Gillilland MG 3rd, Kamada SN, Moon JJ. Hyaluronic acid-bilirubin nanomedicine for targeted modulation of dysregulated intestinal barrier, microbiome and immune responses in colitis. *Nat Mater* 2020;**19**:118–26.
9. Chassaing B, Ley RE, Gewirtz AT. Intestinal epithelial cell toll-like receptor 5 regulates the intestinal microbiota to prevent low-grade inflammation and metabolic syndrome in mice. *Gastroenterology* 2014;**147**:1363–77.e17.
10. Pai YC, Weng LT, Wei SC, *et al*. Gut microbial transcytosis induced by tumor necrosis factor-like 1A-dependent activation of a myosin light chain kinase splice variant contributes to IBD. *J Crohns Colitis* 2021;**15**:258–72.
11. Wu LL, Peng WH, Kuo WT, *et al*. Commensal bacterial endocytosis in epithelial cells is dependent on myosin light chain kinase-activated brush border fanning by interferon-gamma. *Am J Pathol* 2014;**184**:2260–74.
12. Yu LC, Shih YA, Wu LL, *et al*. Enteric dysbiosis promotes antibiotic-resistant bacterial infection: systemic dissemination of resistant and commensal bacteria through epithelial transcytosis. *Am J Physiol Gastrointest Liver Physiol* 2014;**307**:G824–35.
13. Basson AR, Gomez-Nguyen A, Menghini P, *et al*. Human gut microbiome transplantation in ileitis prone mice: a tool for the functional characterization of the microbiota in inflammatory bowel disease patients. *Inflamm Bowel Dis* 2020;**26**:347–59.
14. Torres J, Hu J, Seki A, *et al*. Infants born to mothers with IBD present with altered gut microbiome that transfers abnormalities of the adaptive immune system to germ-free mice. *Gut* 2020;**69**:42–51.
15. Salzman NH, Hung K, Haribhai D, *et al*. Enteric defensins are essential regulators of intestinal microbial ecology. *Nat Immunol* 2010;**11**:76–83.
16. Rehman A, Sina C, Gavrilova O, *et al*. Nod2 is essential for temporal development of intestinal microbial communities. *Gut* 2011;**60**:1354–62.
17. Elinav E, Strowig T, Kau AL, *et al*. NLRP6 inflammasome regulates colonic microbial ecology and risk for colitis. *Cell* 2011;**145**:745–57.
18. Couturier-Maillard A, Secher T, Rehman A, *et al*. NOD2-mediated dysbiosis predisposes mice to transmissible colitis and colorectal cancer. *J Clin Invest* 2013;**123**:700–11.
19. Carvalho FA, Barnich N, Sivignon A, *et al*. Crohn's disease adherent-invasive Escherichia coli colonize and induce strong gut inflammation in transgenic mice expressing human CEACAM. *J Exp Med* 2009;**206**:2179–89.
20. Schmitz JM, Tonkonogy SL, Dogan B, *et al*. Murine adherent and invasive E. coli induces chronic inflammation and immune responses in the small and large intestines of monoassociated IL-10-/- mice independent of long polar fimbriae adhesin A. *Inflamm Bowel Dis* 2019;**25**:875–85.
21. Blair SA, Kane SV, Clayburgh DR, Turner JR. Epithelial myosin light chain kinase expression and activity are upregulated in inflammatory bowel disease. *Lab Invest* 2006;**86**:191–201.
22. Wang F, Graham WV, Wang Y, Witkowski ED, Schwarz BT, Turner JR. Interferon-gamma and tumor necrosis factor-alpha synergize to induce intestinal epithelial barrier dysfunction by up-regulating myosin light chain kinase expression. *Am J Pathol* 2005;**166**:409–19.
23. Cario E, Rosenberg IM, Brandwein SL, *et al*. Lipopolysaccharide activates distinct signaling pathways in intestinal epithelial cell lines expressing Toll-like receptors. *J Immunol* 2000;**164**:966–72.
24. Yu LC, Wei SC, Ni YH. Interplay between the gut microbiota and epithelial innate signaling in colitis-associated colon carcinogenesis. *Cancer Res Frontiers* 2017;**3**:1–28.
25. Fukata M, Chen A, Klepper A, *et al*. Cox-2 is regulated by Toll-like receptor-4 [TLR4] signaling: role in proliferation and apoptosis in the intestine. *Gastroenterology* 2006;**131**:862–77.
26. Chen GY, Shaw MH, Redondo G, Núñez G. The innate immune receptor Nod1 protects the intestine from inflammation-induced tumorigenesis. *Cancer Res* 2008;**68**:10060–7.
27. Scheuerl T, Hopkins M, Nowell RW, Rivett DW, Barraclough TG, Bell T. Bacterial adaptation is constrained in complex communities. *Nat Commun* 2020;**11**:754.
28. Schulte M, Olschewski K, Hensel M. Fluorescent protein-based reporters reveal stress response of intracellular Salmonella enterica at level of single bacterial cells. *Cell Microbiol* 2021;**23**:e13293.
29. Su L, Shen L, Clayburgh DR, *et al*. Targeted epithelial tight junction dysfunction causes immune activation and contributes to development of experimental colitis. *Gastroenterology* 2009;**136**:551–63.
30. Edelblum KL, Sharon G, Singh G, *et al*. The microbiome activates CD4 T-cell-mediated immunity to compensate for increased intestinal permeability. *Cell Mol Gastroenterol Hepatol* 2017;**4**:285–97.
31. Low D, Tran HT, Lee IA, *et al*. Chitin-binding domains of Escherichia coli ChiA mediate interactions with intestinal epithelial cells in mice with colitis. *Gastroenterology* 2013;**145**:602–12.e9.
32. Clark E, Hoare C, Tanianis-Hughes J, Carlson Gordon L, Warhurst G. Interferon gamma induces translocation of commensal Escherichia coli across gut epithelial cells via a lipid raft-mediated process. *Gastroenterology* 2005;**128**:1258–67.
33. Yu LC, Wei SC, Li YH, *et al*. Invasive pathobionts contribute to colon cancer initiation by counterbalancing epithelial antimicrobial responses. *Cell Mol Gastroenterol Hepatol* 2022;**13**:57–79.
34. Grossmann J, Walther K, Artinger M, *et al*. Progress on isolation and short-term ex-vivo culture of highly purified non-apoptotic human intestinal epithelial cells [IEC]. *Eur J Cell Biol* 2003;**82**:262–70.
35. Wu L-L, Chiu H-D, Peng W-H, *et al*. Epithelial inducible nitric oxide synthase causes bacterial translocation by impairment of enterocytic tight junctions via intracellular signals of Rho-associated kinase and protein kinase C zeta. *Crit Care Med* 2011;**39**:2087–98.
36. Huang YJ, Lee TC, Pai YC, Lin B-R, Turner JR, Yu LC. A novel tumor suppressor role of myosin light chain kinase splice variants through downregulation of the TEAD4/CD44 axis. *Carcinogenesis* 2021;**42**:961–74.
37. Chang WY, Yang YT, She MP, *et al*. 5-HT7 receptor-dependent intestinal neurite outgrowth contributes to visceral hypersensitivity in irritable bowel syndrome. *Lab Invest* 2022;**102**:1023–37.

38. Coste A, Dubuquoy L, Barnouin R, *et al*. LRH-1-mediated glucocorticoid synthesis in enterocytes protects against inflammatory bowel disease. *Proc Natl Acad Sci U S A* 2007;**104**:13098–103.
39. Merk VM, Phan TS, Brunner T. Regulation of tissue immune responses by local glucocorticoids at epithelial barriers and their impact on interorgan crosstalk. *Front Immunol* 2021;**12**:672808.
40. Clermont O, Christenson JK, Denamur E, Gordon DM. The Clermont Escherichia coli phylo-typing method revisited: improvement of specificity and detection of new phylo-groups. *Environ Microbiol Rep* 2013;**5**:58–65.
41. Beaumont M, Paes C, Mussard E, *et al*. Gut microbiota derived metabolites contribute to intestinal barrier maturation at the suckling-to-weaning transition. *Gut Microbes* 2020;**11**:1268–86.
42. Pandey U, Aich P. Postnatal intestinal mucosa and gut microbial composition develop hand in hand: a mouse study. *Biomed J* 202216;S2319-4170(22)00033-6.
43. Popoff MR. Bacterial factors exploit eukaryotic Rho GTPase signaling cascades to promote invasion and proliferation within their host. *Small GTPases* 2014;**5**:e983863.
44. Huang YJ, Pai YC, Yu LC. Host-microbiota interaction and intestinal epithelial functions under circadian control: implications in colitis and metabolic disorders. *Chin J Physiol* 2018;**61**:325–40.
45. Froy O, Chapnik N. Circadian oscillation of innate immunity components in mouse small intestine. *Mol Immunol* 2007;**44**:1954–60.
46. Sladek M, Rybova M, Jindrakova Z, *et al*. Insight into the circadian clock within rat colonic epithelial cells. *Gastroenterology* 2007;**133**:1240–9.
47. Simon AR, Vikis HG, Stewart S, Fanburg BL, Cochran BH, Guan KL. Regulation of STAT3 by direct binding to the Rac1 GTPase. *Science* 2000;**290**:144–7.
48. Inczefi O, Bacquie V, Olier-Pierre M, *et al*. Targeted intestinal tight junction hyperpermeability alters the microbiome, behavior, and visceromotor responses. *Cell Mol Gastroenterol Hepatol* 2020;**10**:206–8.e3.
49. Chen TL, Chen S, Wu HW, *et al*. Persistent gut barrier damage and commensal bacterial influx following eradication of Giardia infection in mice. *Gut Pathog* 2013;**5**:26.
50. Kalischuk LD, Leggett F, Inglis GD. Campylobacter jejuni induces transcytosis of commensal bacteria across the intestinal epithelium through M-like cells. *Gut Pathog* 2010;**2**:14.
51. Wang A, Keita AV, Phan V, *et al*. Targeting mitochondria-derived reactive oxygen species to reduce epithelial barrier dysfunction and colitis. *Am J Pathol* 2014;**184**:2516–27.
52. Lewis K, Lutgendorff F, Phan V, *et al*. Enhanced translocation of bacteria across metabolically stressed epithelia is reduced by butyrate. *Inflamm Bowel Dis* 2010;**16**:1138–48.
53. Lopes F, Keita AV, Saxena A, *et al*. ER-stress mobilization of death-associated protein kinase-1-dependent xenophagy counteracts mitochondria stress-induced epithelial barrier dysfunction. *J Biol Chem* 2018;**293**:3073–87.
54. Saxena A, Lopes F, McKay DM. Reduced intestinal epithelial mitochondrial function enhances in vitro interleukin-8 production in response to commensal Escherichia coli. *Inflamm Res* 2018;**67**:829–37.
55. Lu L, Xu W, Liu J, *et al*. DRG1 maintains intestinal epithelial cell junctions and barrier function by regulating RAC1 activity in necrotizing enterocolitis. *Dig Dis Sci* 2021;**66**:4237–50.
56. den Hartog G, Butcher LD, Ablack AL, *et al*. Apurinic/apyrimidinic endonuclease 1 restricts the internalization of bacteria into human intestinal epithelial cells through the inhibition of Rac1. *Front Immunol* 2020;**11**:553994.
57. Palmieri O, Mazzoccoli G, Bossa F, *et al*. Systematic analysis of circadian genes using genome-wide cDNA microarrays in the inflammatory bowel disease transcriptome. *Chronobiol Int* 2015;**32**:903–16.
58. Oh SK, Kim D, Kim K, *et al*. RORalpha is crucial for attenuated inflammatory response to maintain intestinal homeostasis. *Proc Natl Acad Sci U S A* 2019;**116**:21140–9.
59. Stokes K, Cooke A, Chang H, Weaver DR, Breault DT, Karpowicz P. The circadian clock Gene BMAL1 coordinates intestinal regeneration. *Cell Mol Gastroenterol Hepatol* 2017;**4**:95–114.
60. Tuganbaev T, Mor U, Bashiardes S, *et al*. Diet diurnally regulates small intestinal microbiome-epithelial-immune homeostasis and enteritis. *Cell* 2020;**182**:1441–59.e21.
61. Leone V, Gibbons SM, Martinez K, *et al*. Effects of diurnal variation of gut microbes and high-fat feeding on host circadian clock function and metabolism. *Cell Host Microbe* 2015;**17**:681–9.
62. Wang Y, Kuang Z, Yu X, Ruhn KA, Kubo M, Hooper LV. The intestinal microbiota regulates body composition through NFIL3 and the circadian clock. *Science* 2017;**357**:912–6.
63. Thaiss CA, Levy M, Korem T, *et al*. Microbiota diurnal rhythmicity programs host transcriptome oscillations. *Cell* 2016;**167**:1495–510.e12.